Available online at www.sciencedirect.com
SCIENCE DIRECT®
Geochimica et Cosmochimica Acta 70 (2006) 1796–1806
Geochimica
www.elsevier.com/locate/gca

Experimental determination of the solubility of natural wollastonite in pure water up to pressures of 5 GPa and at temperatures of 400–800 °C

Thomas Fockenberg *, Michael Burchard, Walter V. Maresch

Institut für Geologie, Mineralogie und Geophysik, Ruhr-Universität Bochum, D-44780 Bochum, Germany

Received 13 December 2004; accepted in revised form 29 December 2005

Abstract

The solubility of natural, near-end-member wollastonite-I (>99.5% $CaSiO_3$) has been determined at temperatures from 400 to 800 °C and pressures between 0.8 and 5 GPa in piston-cylinder apparatus with the weight-loss method. Chemical analysis of quench products and optical monitoring in a hydrothermal diamond anvil cell demonstrates that no additional phases form during dissolution. Wollastonite-I, therefore, dissolves congruently in the pressure–temperature range investigated. The solubility of $CaSiO_3$ varies between 0.175 and 13.485 wt% and increases systematically with both temperature and pressure up to 3.0 GPa. Above 3.0 GPa wollastonite-I reacts rapidly to the high-pressure modification wollastonite-II. No obvious trends are evident in the solubility of wollastonite-II, with values between 1.93 and 10.61 wt%. The systematics of wollastonite-I solubility can be described well by a composite polynomial expression that leads to isothermal linear correlation with the density of water. The molality of dissolved wollastonite-I in pure water is then

$$\log(m_{\mathrm{woll}}) = 2.2288 - 3418.23 \times T^{-1} + 671386.84 \times T^{-2} + \log \rho_{\mathrm{H_2O}} \times (5.4578 + 2359.11 \times T^{-1}).$$

By combining the present experimental data with literature data on the solubility of quartz (Manning, C.E., Boettcher, S.L., 1994. Rapid-quench hydrothermal experiments at mantle pressures and temperatures. *Am. Mineral.* **79**, 1153–1158.) and wollastonite-I + quartz (Xie, Z., Walther, J.V., 1993b. Wollastonite + quartz solubility in supercritical NaCl aqueous solutions. *Am. J. Sci.* **293**, 235–255.) in pure water, an analogous expression can be derived for the solubility of wollastonite in quartz-saturated aqueous solution as follows:

$$\log(m_{\mathrm{woll}}) = 2.5930 - 3660.98 \times T^{-1} + 671402.32 \times T^{-2} + \log \rho_{\mathrm{H_2O}} \times (-1.3609 + 6775.13 \times T^{-1}). \quad (\text{all temperatures are in}^{\circ}\mathrm{C})$$

This expression adequately describes wollastonite-I solubility between 0.2–3 GPa and 300–800 °C.

1. Introduction

Fluids ranging from hydrous melts to dense aqueous and CO_2-rich solutions play a major role in the petrology and ductile behaviour of rocks in the deeper levels of the crust or of crustal rocks subducted into the upper mantle (e.g., Manning, 2004). In addition, data on the solubility of minerals in aqueous solutions at high pressures are essential for an understanding of fluid properties, mass transport and growth/dissolution processes of minerals in the Earth's crust and upper mantle. Although work on this topic has been accelerating during the last few years, experimental data on a very large number of important rock-forming minerals and mineral assemblages are still lacking. Dykes and veins rich in SiO_2, presumably representing precipitates from high-temperature, high-pressure aqueous solutions or hydrous melts, are common in many lower crustal metamorphic rocks. As a result, many experimental studies have been carried out in the relatively simple system SiO_2-H_2O, and systematic data for pressures up to 2 GPa and temperatures up to 900 °C are now available (see

* Corresponding author. Fax: +49 0 234 32 14433.
E-mail address: thomas.fockenberg@rub.de (T. Fockenberg).

0016-7037/$ - see front matter © 2006 Elsevier Inc. All rights reserved.
doi:10.1016/j.gca.2005.12.017

summaries by Manning, 1994, 2004; Gerya et al., 2005). Some data on SiO_2-solubility in more complex fluids involving CO_2 and/or NaCl are also available (e.g., Xie and Walther, 1993a; Newton and Manning, 2000). Experiments on the solubility of wollastonite-I or wollastonite-I + quartz, either in pure water or more complex solutions involving NaCl or $CaCl_2$, are limited to 0.2 GPa or less (e.g., Gunter and Eugster, 1978; Popp and Frantz, 1979; Xie and Walther, 1993a,b). A number of studies have dealt with the dissolution of wollastonite-I in pure water at 1 bar (Bailey and Reesman, 1971; Rimstidt and Dove, 1986; Casey et al., 1993; Xie and Walther, 1994; Weissbart and Rimstidt, 2000), but these results generally reflect non-equilibrium processes. Experimental solubility data on important Ca-rich phases, either in pure water or aqueous solutions with NaCl and/or HCl, have also been presented by Eggler and Rosenhauer (1978) for diopside, by Roselle and Baumgartner (1995) for anorthite, by Walther (1986) and Seewald and Seyfried (1991) for portlandite, and by Fein and Walther (1987, 1989a), Newton and Manning (2002) as well as Caciagli and Manning (2003) for calcite. In addition to these experimental studies, attempts have also been made to compute the solubility of rock-forming minerals (Franz et al., 1981; Walther, 1986), leading to data compilations on equilibrium constants of selected mineral—fluid equilibria at pressures up to 200 MPa, mostly in the presence of dissolved chlorides.

In this paper we present new data on the solubility of natural wollastonite-I ($CaSiO_3$) in pure supercritical water in the pressure range 0.8–5.0 GPa and at temperatures between 400 and 800 °C. In accordance with the phase diagram of Huang and Wyllie (1975), a transformation from the natural low-pressure polymorph wollastonite-I to wollastonite-II was observed at pressures between 3.5 and 4.0 GPa. This study considerably extends the pressure and temperature range of existing solubility measurements of wollastonite in pure H_2O. This paper initiates our reports on a systematic series of high-pressure solubility studies that have been undertaken on minerals in the system K_2O-CaO-MgO-Al_2O_3-SiO_2-H_2O.

2. Previous studies on wollastonite

Wollastonite-I (hereafter written as the binary oxide $CaSiO_3$ rather than the structural formula $Ca_3[Si_3O_9]$) is a relatively common chain silicate in nature, and has the advantage of being chemically simple and often of very high purity. It is thus an excellent starting point for systematic studies on the solubilities of rock-forming minerals. Xie and Walther (1993b) studied the solubility of wollastonite-I + quartz at temperatures up to 650 °C and pressures of 100 and 200 MPa in fluids ranging from pure water to solutions of NaCl in water at various concentrations. The fluids were isolated at high temperatures and pressures with an extraction-quench hydrothermal apparatus and analyzed by DCP emission spectrometry. In pure water, the concentration of Si was found to be comparable to that of quartz in pure water, increasing with increasing pressure and temperature. However, Ca was found to exhibit a quite different behaviour. At temperatures below about 500 °C the concentration of Ca decreases with increasing temperature; above 500 °C it increases. The molality of calcium in the solution is about 100 times lower than that of Si.

Because Xie and Walther (1993b) focused on the solubility of wollastonite-I + quartz, these experiments yield no direct information on congruent vs. incongruent dissolution behaviour of pure wollastonite-I in H_2O. A number of studies on wollastonite-I dissolution behaviour have been carried out at 1 bar. However, the major issue in most of these studies is the stoichiometry and rate of the dissolution mechanism and not the attainment of an equilibrium state between the mineral and aqueous fluid. Bailey and Reesman (1971), Casey et al. (1993), Xie and Walther (1994) as well as Weissbart and Rimstidt (2000) studied the reaction between water and wollastonite-I at 1 bar pressure and concluded that wollastonite-I dissolves incongruently, i.e. non-stoichiometrically. In contrast, Rimstidt and Dove (1986) interpreted results from mixed-flow reactor experiments on wollastonite-I–H_2O to indicate congruent, stoichiometric solution behaviour. Generally, even at room temperature (e.g., Xie and Walther, 1994), it was found that the rate of removal of Ca from crystal surfaces is much higher than that for Si, suggesting that Ca is more loosely bonded than Si. Casey et al. (1993) used high-resolution transmission electron microscopy to show details of the wollastonite-I dissolution process in water. Calcium is quickly removed from the outer surface of wollastonite-I crystals, and hydrogen ions protonate the remaining oxygens. Then two hydroxyl groups react to produce H_2O, and the newly formed very stable siloxane Si-O-Si bridges form a restructured, Si-rich near-surface region that retards further dissolution of the wollastonite-I crystal.

Few determinations exist on the actual speciation of dissolved silicon and calcium in pure water at elevated pressures. Zotov and Keppler (2000, 2002) interpreted in situ Raman spectra obtained on SiO_2-H_2O solutions at pressures up to 1.4 GPa and temperatures up to 900 °C to indicate increasing polymerization of H_4SiO_4 monomer to $H_6Si_2O_7$ dimer aqueous silicate species with increasing pressure. In contrast, Davis et al. (2001) report from an analogous study up to 1.4 GPa and 700 °C that, at constant dissolved silica content and increasing pressure, the intensity of the dimer Raman bands increases whereas the intensity of the monomer bands remains constant. Doltsinis et al. (2004) have recently pointed out that such discrepancies could be due to the inherent difficulties in interpreting experimental Raman spectra from aqueous solutions. Nevertheless, recent solubility studies by direct methods (Zhang and Frantz, 2000; Newton and Manning, 2002, 2003) concur that increasing polymerization of SiO_2 in aqueous fluid can become significant at elevated pressures and temperatures. Gerya et al. (2005) modeled the existing experimental data on SiO_2 solubility in H_2O using

a new thermodynamic approach for describing H_2O as a function of pressure and temperature. They conclude that dissolved silica in quartz-buffered aqueous solutions is considerably polymerized, exceeding 20–25% at all temperatures above 400 °C.

Roselle and Baumgartner (1995) suggest the presence of $Ca(OH)^+$ complexes for dissolved Ca at 200 MPa and 400–600 °C. Fein and Walther (1987) and Xie and Walther (1993b), on the other hand, concluded that Ca^{2+} should be the dominant species at such P-T conditions. In their study on the solubility of calcite in water at 0.6–1.6 GPa and 500–800 °C, Caciagli and Manning (2003) interpreted their data primarily on the basis of Ca^{2+}, but concluded that $Ca(OH)^+$ could also be an important calcium species. Other studies on the solubility of wollastonite-I (e.g., Gunter and Eugster, 1978) and other Ca-bearing phases like calcite and portlandite (Fein and Walther, 1989a,b) were carried out predominantly in the presence of chloride ions. Because Ca forms chloride complexes in such saline solutions (e.g., Franz et al., 1981), these results are not pertinent to the present study.

3. Experimental techniques

A natural wollastonite-I single crystal from Kropfmühl (Bavarian Forest, Germany) served as starting material. Electron microprobe analysis (CAMECA SX 50, Ruhr-University of Bochum) yields $Ca_{0.994}Fe_{0.003}Mn_{0.003}SiO_3$. Some very small (<20 μm) garnet crystals were detected as inclusions within the wollastonite-I crystal, but the relative amount by volume is so extremely small that the effect on the solubility determinations of wollastonite-I is assumed to be negligible. Because of the excellent cleavage of wollastonite-I, we used cleavage fragments of a large single crystal. These were cleaned in ethanol for several minutes to remove impurities from the surface; their quality was checked optically. Cleavage fragments between 4 and 42 mg were loaded in small gold capsules (inner diameter 4 mm; length 9 mm; wall thickness 0.5 mm), which were then filled completely with doubly distilled, deionized water. Care was taken that no air bubbles were present in the capsule containing the crystal fragment. A second larger gold capsule was slipped over these containers, with the inner diameter of the second capsule chosen so as to provide a tightly fitting sleeve. A small gold disk protected the seat of the inner smaller capsule during crimping and cold-welding of the outer capsule. With this novel procedure, it was possible to minimize the loss of water during the cold-welding process. The weight of the sample and of the gold capsules was monitored on a microbalance after each step of the sample preparation procedure.

Runs were performed in a piston-cylinder apparatus using rock salt and pyrophyllite as pressure media. Temperatures were measured with a chromel–alumel thermocouple, taking into account the corrections for the pressure dependence of the e.m.f.. Further details are given in Fockenberg (1998). As described by Becker et al. (1983) in their determination of the solubility of corundum, loss of water from water-rich capsules can occur during the compressional phase in piston-cylinder apparatus through very small leaks in the welded capsule, i.e., before the sample assembly begins to flow and equilibrate to a quasi-hydrostatic state. To minimize such losses, we approached the required run conditions by pressurizing at room temperature before heating to run conditions. All solubility determinations are based on the amount of water in the capsule after the run (e.g., Table 1). At the end of each run the power was switched off, and cooling to below 200 °C was accomplished in about 20 s. In agreement with Manning (1994), we found that these quench rates are high enough to provide reliable and reproducible results. Run times were between 5 and 241 h (Table 1), which, according to Manning (1994) and Xie and Walther (1993b), are sufficient to ensure equilibrium. After the runs each capsule was cleaned from adhering pyrophyllite, carefully reweighed and punctured using an extracting vessel analogous to that described by Manning and Boettcher (1994). The punctured capsule was dried at 60 °C for 8 h, again reweighed, opened with a small saw and inspected under a binocular microscope. To determine the weight loss of the wollastonite-I the undissolved rest of the single crystal fragments was carefully cleaned from precipitated material with a scalpel and then reweighed. Because quench material was generally not found to adhere to the original crystal (see Fig. 1), this procedure proved to be adequate, without further potentially distorting procedures of leaching or mechanical abrasion. Experimental errors are ±2% for the stated pressures and ±3% for the temperatures (see Fockenberg, 1998). The microbalance yields an error of 0.01 mg for each mass determination. On the basis of these predictable sources of possible error, an accuracy of ±0.3 wt% appears theoretically attainable, but comparison of results at identical P-T conditions (e.g., Table 1) shows that the scatter of the data exceeds this range, even for runs with no recognizable irregularities during the experiment. Seven replicate experiments at 700 °C/2 GPa range between 0.415 and 1.445 wt% wollastonite solubility. No trend as a function of run time was observed between 5 and 212 h, corroborating the conclusions of Manning (1994) as well as Xie and Walther (1993b) that short run times of several hours are enough to reach equilibrium in the capsules.

To monitor the solubility behaviour of wollastonite-I qualitatively, additional experiments were carried out in a hydrothermal diamond anvil cell up to 4.0 GPa and 800 °C. This particular cell type is equipped with a special spring construction to minimize gasket deformation and to allow routine experiments up to 4.5 GPa and 900 °C (Burchard et al., 2003). Temperatures were determined with two type-K thermocouples with a very small diameter of 25 μm, which had previously been calibrated against a diamond anvil equipped with integrated thermosensors (Zaitsev et al., 2001). The pressure was estimated from

Table 1
Experimental results

Run no.	T/°C	P/GPa	Duration/h	w H_2O (i)/mg	w H_2O (f)/mg	w wo. (i)/mg	w wo. (f)/mg	Solubility (wt%)	$\log(m_{woll\ (aq)})$	$m_{woll\ (aq)}$
QL-72	700	0.8	70	153.581	133.953	14.305	14.070	0.175	−1.8210	0.0151
QL.52	500	1.0	66	117.171	97.246	5.798	5.568	0.236	−1.6904	0.0204
QL-108	500	1.0	118	88.780	81.066	8.278	8.028	0.241	−1.6820	0.0208
QL-53	600	1.0	119	109.953	84.807	4.334	4.258	0.185	−1.7990	0.0159
QL-54X	700	1.0	67	89.210	66.098	6.717	6.184	0.798	−1.1590	0.0690
QL-59	700	1.0	68	131.709	127.783	9.143	8.622	0.406	−1.4550	0.0353
QL-77	800	1.0	70	94.803	74.453	23.301	22.548	1.001	−1.0600	0.0871
QL-48	600	1.4	44	100.600	79.374	13.780	13.082	0.872	−1.1210	0.0757
QL-51	500	1.5	70	92.111	65.308	11.308	11.024	0.433	−1.4270	0.0374
QL-120	600	1.5	241	102.330	92.355	18.460	17.558	0.967	−1.0752	0.0841
QL-50	700	1.5	39	95.776	80.912	3.396	2.916	0.590	−1.2920	0.0511
QL-107	700	1.5	89	102.502	84.656	6.206	5.822	0.452	−1.4090	0.0390
QL-119X	700	1.5	63	95.232	83.106	50.452	48.646	2.127	−0.7280	0.1870
QL-74X	800	1.5	88	127.548	127.348	14.858	12.080	2.130	−0.8420	0.1440
QL-79	400	2.0	142	110.084	108.420	21.058	20.474	0.536	−1.3336	0.0464
QL-56	500	2.0	91	107.767	99.853	9.377	8.728	0.646	−1.2520	0.0560
QL-57	600	2.0	94	96.443	78.381	8.765	7.763	1.262	−0.9580	0.1101
QL-99	600	2.0	95	107.214	94.566	13.680	12.876	0.843	−1.1350	0.0732
QL-123	600	2.0	95	109.394	98.388	10.764	9.962	0.809	1.1150	0.0702
QL-58X	700	2.0	70	125.893	123.609	12.841	9.670	2.501	−0.7590	0.1740
QL-122X	700	2.0	161	102.808	77.692	26.744	24.494	2.815	−0.6030	0.2490
QL-103	700	2.0	5	81.468	65.890	17.938	17.412	0.792	−1.1630	0.0687
QL-100	700	2.0	42	85.932	71.986	13.292	12.992	0.415	−1.4450	0.0359
QL-105	700	2.0	67	106.196	99.936	10.556	9.832	0.719	−1.2050	0.0624
QL-106	700	2.0	69	111.594	107.678	6.656	5.650	0.926	−1.0950	0.0804
QL-102	700	2.0	112	103.118	82.298	17.984	17.438	0.659	−1.2430	0.0571
QL-98	700	2.0	119	85.660	77.866	42.002	40.860	1.445	−0.8990	0.1263
QL-101	700	2.0	212	76.860	75.434	14.440	13.810	0.828	−1.1430	0.0719
QL-60X	800	2.0	69	116.921	114.045	6.017	4.282	1.626	−0.8470	0.1423
QL-61	800	2.0	68	129.920	109.752	6.585	3.228	2.970	−0.5800	0.2630
QL-118	600	2.5	112	100.269	90.896	14.564	11.672	3.084	−0.5620	0.2739
QL-117	700	2.5	45	112.258	108.352	14.426	8.708	5.013	−0.3427	0.4543
QL-124	700	2.5	97	102.378	84.376	36.664	33.710	3.383	−0.5210	0.3014
QL-85	500	3.0	93	110.020	66.940	17.084	4.397	2.590	−0.6400	0.2289
QL-86X	700	3.0	70	87.723	71.987	13.307	4.476	10.927	0.0237	1.0561
QL-110	700	3.0	96	111.814	72.384	6.846	2.128	6.119	−0.2510	0.5611
QL-75	800	3.0	47	119.659	98.613	22.593	7.222	13.485	0.1280	1.3418
QL-83	500	4.0	22	99.452	80.174	43.730	38.978	5.595	−0.2922	0.5103
QL-87	600	4.0	120	117.091	60.723	15.757	10.134	8.475	−0.0985	0.7970
QL-91	700	4.0	61	118.483	95.742	10.696	5.146	5.480	−0.3019	0.4990
QL-93	800	4.0	63	110.950	90.282	22.852	16.352	6.716	−0.2077	0.6198
QL-64	500	5.0	71	120.346	62.182	27.098	20.366	9.769	−0.0310	0.9320
QL-84	500	5.0	45	120.034	102.962	14.532	2.946	10.159	−0.0117	0.9735
QL-69	600	5.0	85	120.655	101.475	26.349	14.300	10.610	0.0090	1.0222
QL-73	700	5.0	70	118.009	85.874	14.047	10.836	3.600	−0.4920	0.3219
QL-66	800	5.0	46	125.395	113.793	20.409	18.172	1.930	−0.0772	0.1690
QL-71	800	5.0	46	113.744	93.708	17.590	12.982	4.690	−0.3730	0.4233

X, run not considered during data regression (see text). w, weight; i, initial; f, final; m, molality.

the equation of state of H_2O (Halbach and Chatterjee, 1982). The sample volume remains nearly constant up to 700 °C before it begins to decrease slowly. The wollastonite-I to wollastonite-II transition between 3.5 and 4.0 GPa (Huang and Wyllie, 1975) provides a convenient calibration point. The phase contents of the cell were checked qualitatively with a Labram Raman spectrometer with a Laser wave length of 514 nm.

To determine whether the quenched crystals of high-pressure runs in the piston-cylinder apparatus were wollastonite-I or -II after the run, several crystals were crushed, powdered and then X-rayed with Cu Kα radiation on a PHILIPS PW 1710 powder diffractometer. Chemical analyses were performed with a CAMECA SX 50 electron microprobe. The acceleration voltage was 15 kV and the beam current 10 nA. A glass of wollastonite composition

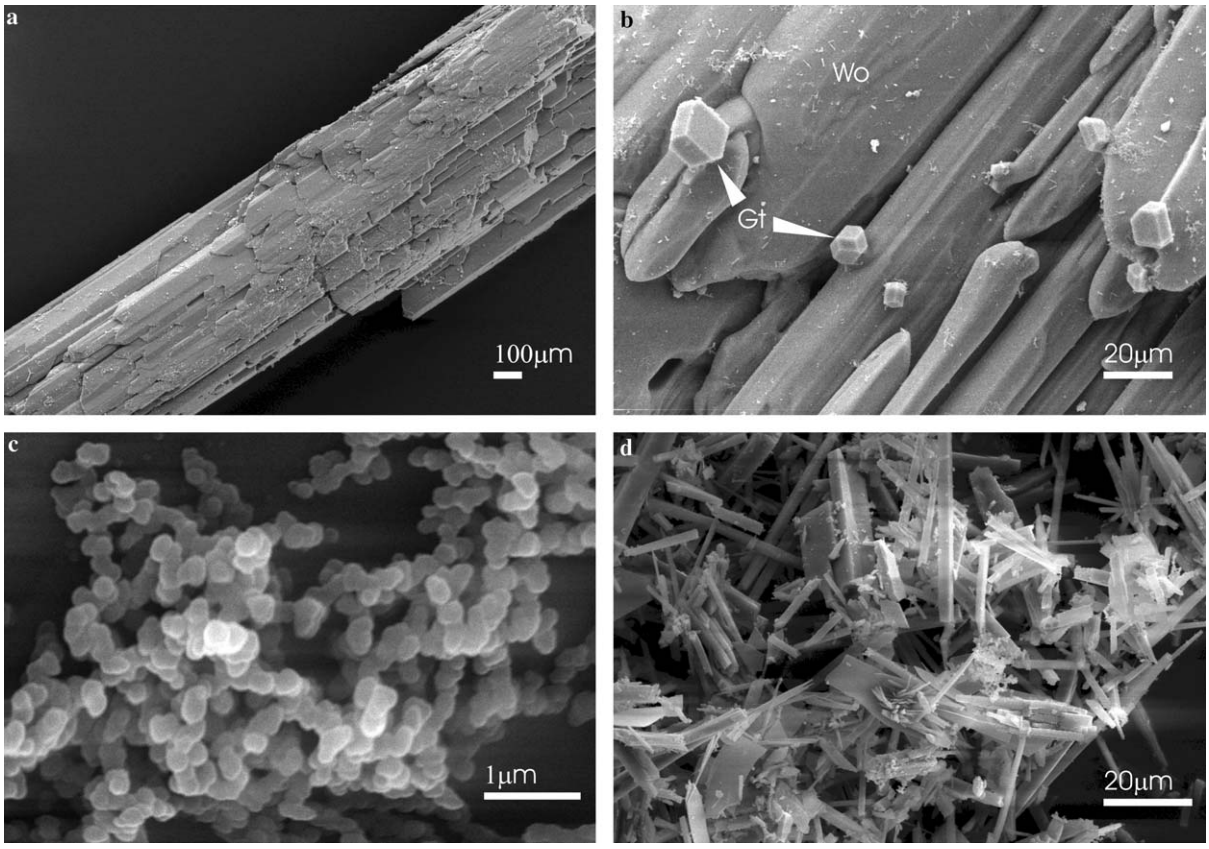

Fig. 1. Scanning electron microscope images of capsule contents after quenching and drying. (a) General view of wollastonite surface of partially dissolved crystal after the experiment. (b) Detail of wollastonite crystal after the experiment. Note etch grooves localized by cleavage planes and small garnet crystals accumulated at the surface due to dissolution of the wollastonite host. (c) Globules of quench material precipitated from the solution saturated with calcium silicate. (d) Aggregates of wollastonite crystals found in some runs at 4.0 and 5.0 GPa.

(Ca, Si), andradite (Fe) and spessartine (Mn) served as standards. Microphotographs and qualitative chemical analyses were obtained with a LEO 1530 scanning electron microscope. Both instruments are provided by the Ruhr-University of Bochum.

4. Experimental results

Experiments were performed between 400 and 800 °C and at pressures ranging from 0.8 to 5.0 GPa. All run data and experimental results are summarized in Table 1. Despite the high pressures and the relatively large volumes of water involved, the gold capsules were only very slightly and homogeneously deformed at the end of the runs. The fluid observed during opening of the capsules was clear for runs at lower pressures and temperatures and became milky for runs at higher P-T conditions. This appearance is obviously correlated with the degree of wollastonite solubility achieved. At high solubilities, some of the originally dissolved material fails to reprecipitate during quenching and remains as a colloid in the fluid. After drying, inspection of the two halves of the gold capsules with a binocular microscope showed that at pressures up to and including 3.0 GPa the initial crystal could easily be detected and removed with small tweezers. In several runs above 3.0 GPa the crystal appeared shattered and disaggregated; no reliable solubility calculations were possible from such experiments. In most cases the crystals were translucent to slightly milky in appearance and covered with only a small amount of quenched material (Figs. 1a and b), an observation also reported by Rimstidt and Dove (1986). The edges and the relatively sharp cleavage contours of the original crystal fragments become more subdued and rounded. Elongated etch pits appear to be localized by the prominent cleavage of wollastonite-I (Fig. 1b). Small idiomorphic garnets were observed on the surface of the dissolving wollastonite-I fragments which were already present as inclusions in the starting material (see above). Chemical analysis shows that these crystals are close to andradite in composition, with about 10 mol% grossular component (Table 2). Because of the low amounts of garnet involved (we estimate less than 0.1 wt% garnet), no attempt was made to consider garnet solubility.

The precipitation of new wollastonite-I on the original crystal was never observed (Figs. 1a and b). Although dissolution proceeds preferentially along cleavage planes, leading to a "dissected" appearance of the surface (Fig. 1b), recognizable crystal faces develop. These become more and more prominent at higher temperatures and

Table 2
Selected electron microprobe data of wollastonite-I, garnet and quench material

	SiO_2	Al_2O_3	FeO	Fe_2O_3	MnO	CaO	Sum	Si	Al	Fe^{2+}	Fe^{3+}	Mn	Ca
Starting material	51.37	—	0.09	—	0.02	48.51	99.99	3.02	—	0.005	—	0.001	2.99
	51.98	—	0.02	—	0.00	48.47	100.54	3.00	—	0.001	—	0.000	3.00
	51.75	—	0.14	—	0.06	49.14	101.11	3.03	—	0.007	—	0.003	2.98
	51.79	—	0.08	—	0.00	48.87	100.84	3.02	—	0.004	—	0.000	2.99
Woll-I (run QL-51)	51.11	—	0.08	—	0.00	47.91	99.18	2.99	—	0.004	—	0.000	3.01
	50.97	—	0.04	—	0.01	47.64	98.76	3.00	—	0.002	—	0.001	3.00
	52.30	—	0.03	—	0.00	48.81	101.21	3.00	—	0.002	—	0.000	3.00
Quench material (run QL-48)	50.91	—	0.23	—	0.25	48.15	99.70	2.97	—	0.011	—	0.012	3.02
	51.00	—	0.15	—	0.28	47.75	99.27	2.99	—	0.007	—	0.014	3.00
Quench material (run QL-66)	50.87	—	0.20	—	0.38	47.83	99.28	2.98	—	0.011	—	0.020	3.01
	51.31	—	0.17	—	0.34	49.53	101.35	2.96	—	0.008	—	0.017	3.05
	49.43	—	0.14	—	0.26	43.85	93.79	3.04	—	0.007	—	0.014	2.89
	50.71	—	0.23	—	0.77	48.18	99.99	2.96	—	0.011	—	0.038	3.02
Garnet (run QL-64)	37.12	3.28	—	25.87	0.10	34.21	100.58	3.02	0.36	—	1.61	0.007	3.00
	35.29	0.58	—	30.57	0.10	33.84	100.28	2.97	0.06	—	1.93	0.007	3.05
	36.46	1.73	—	28.22	0.15	33.75	100.51	3.02	0.19	—	1.78	0.010	3.00

Oxides in wt%. Cation proportions on the basis of 9 oxygens except garnet (12 oxygens).

pressures. The precipitated phases covering the walls of the gold capsules are easily scratched off with a needle. All solid phases recovered after drying were weighed separately, and the sum approximates the initial weight of the single crystal. The precipitated material consists almost entirely of rounded dull-white globules (Fig. 1c) with a diameter of less than 3 μm; occasionally a few shiny needles of newly grown wollastonite-I were observed, as corroborated by energy-dispersive analysis with the scanning electron microscope. The two phases can be readily distinguished macroscopically on the basis of their differing brightness; in addition, the newly formed crystals are translucent in contrast to the starting material.

In several runs at 700 and 800 °C, irregularities during the experiment and/or difficulties in interpreting the quenched material unequivocally led us to disregard these data during later considerations of wollastonite solubility systematics. Such runs are marked by "X" in Table 1. In run QL-119, the original crystal was broken into a number of small fragments. In runs QL-54, 58, 74 and 122 a large number of small translucent needles appeared as solid phases in the run product. As these small needles are intimately intergrown with the globules, they could logically be interpreted as quenched material. On the other hand, it seems doubtful whether such crystals could really have grown during the short time interval of the quench process. All these runs lead to unusually high calculated amounts of dissolved wollastonite and were not considered further. In run QL-60 uncontrolled decompression occurred during the run. Some translucent and separable crystals observed in run QL-86 appear to have formed during the experiment, perhaps in response to an aberrantly high thermal gradient in the capsule. Thus, the comparatively high value of 10.927 wt% dissolved wollastonite seems to be doubtful.

At 5.0 GPa the precipitated material forms a framework covering the whole capsule, and aggregates of small idiomorphic wollastonite-I and -II crystals are particularly prominent (Fig. 1d). Although it cannot be completely ruled out that these crystals could represent fragments of the original crystal broken off during pressurization of the run, their habit suggests that they crystallized from the fluid during the run. It also appears doubtful that such idiomorphic crystals could have formed during the quench phase. An origin due to solution/reprecipitation processes caused by thermal gradients in the capsule or due to the recrystallization from wollastonite-I to wollastonite-II above 3.0 GPa (see below) appears likely. Nevertheless, the weight of these crystals is very low in comparison to that of the unambiguous quench material represented by the milky spheres, so that any possible resultant error in the determination of wollastonite solubility should be minor.

Apart from the garnet already present in the starting material, no phases other than quench products and wollastonite were encountered, thus suggesting congruent dissolution of the wollastonite-I starting material at the P-T conditions of the present study. To further corroborate this conclusion, comparative chemical analyses on starting material and precipitated products were attempted with the electron microprobe. Table 2 lists analyses of the starting material, the remaining wollastonite-I fragment from run QL-51 (1.5 GPa, 500 °C) and the quenched material from runs QL-48 (1.5 GPa, 600 °C) and QL-66 (5 GPa, 800 °C). The latter runs were chosen because the amount of quenched material was large enough to allow preparation for electron microprobe analysis. The results indicate that, within error, there are no significant differences in the Ca/Si ratios, even in the case of run QL-66 which was run within the wollastonite-II stability field. The slight enrichment of Fe and Mn in the quench phase can be related to the garnet impurity. To check that at a given pressure and temperature no other phases were formed, we used the diamond anvil cell as an alternative experimental method.

Raman spectroscopy revealed no additional solid phases within the run up to 4.0 GPa and 750 °C. Thus, we conclude from all these observations that in our study wollastonite-I appears to have dissolved congruently in pure water. The same may be true in the case of wollastonite-II. Although this conclusion appears to be in contrast to the observations reported by Rimstidt and Dove (1986), who suggested incongruent dissolution behaviour of wollastonite at low pressures, it must be emphasized that these authors carried out their experiments in a flow reactor. No direct comparison to our runs under steady state conditions can be made.

Fig. 2 summarizes the solubility data for wollastonite-I up to 3.0 GPa in terms of the logarithm of the molality of dissolved wollastonite, because this is the variable that will be used in further discussions. The solubility of wollastonite-I increases with both increasing temperature and pressure. The maximum solubility determined is approximately 14 wt% at 3.0 GPa and 800 °C, equivalent to a 1.34 molal solution. The data scatter is ±0.2 to 0.3 log units. The seven replicate analyses at 700 °C/2 GPa lead to a 1 standard deviation of 0.28 log units. Despite the relatively large scatter in the data, which must be due to additional inherent uncertainties in pressure- and temperature-control in the piston-cylinder assembly, as well as handling problems with the run products, the solubility trends are systematic, even at lower pressures.

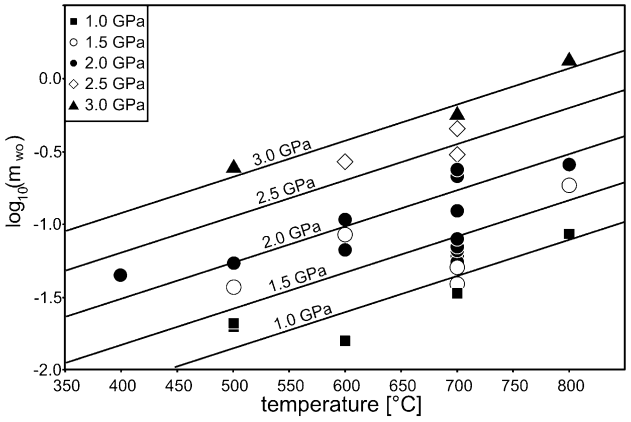

Fig. 2. Summary of experimentally determined solubility of wollastonite-I in water in terms of the logarithm of wollastonite molality, $CaSiO_3$ (see Table 1). The size of the symbols indicates the theoretically attainable accuracy of the experimental method, but the actual scatter in the data is ±0.2 to 0.3 log units. The isobars are simple eye-ball fits to the data surface in solubility-temperature–pressure space to guide the eye. A template for assessing solubility systematics in presented in conjunction with Fig. 4.

According to Huang and Wyllie (1975), the stability field of the high pressure polymorph wollastonite-II should be encountered at pressures between 4.0 and 3.5 GPa for temperatures of 200–800 °C, respectively. The transformation is first order. Whereas wollastonite I possesses the well-known classical *dreier* single-chain structure, wollastonite-II is a ring silicate (Trojer, 1969). X-ray powder diffraction of the crystal fragments recovered from experiments at 4.0 and 5.0 GPa show that these indeed possess wollastonite-II structure. Furthermore, we were able to observe the reaction from wollastonite-I to wollastonite-II in situ with the diamond anvil cell (Fig. 3). It is very fast (<1 min) in the temperature range of the present study. This is consistent with the observation of Huang and Wyllie (1975), who, although their experiments were carried out at higher temperatures, observed that wollastonite-I had reacted completely to wollastonite-II in runs of only a few minutes. Fig. 3 indicates that single crystals of wollastonite-I are replaced by aggregates of wollastonite-II, providing a logical explanation for the fact that in runs above 3.0 GPa in the piston-cylinder apparatus the original single wollastonite-I crystal was commonly transformed into several new crystals of various sizes. Accurate determination of weight loss is thus not feasible, despite the fact that, although wollastonite-I was used as starting material, the solubility data at 4.0 and 5.0 GPa (Table 1) could in principle be directly applied to wollastonite-II. Indeed, the experimental results for wollastonite-II fail to yield the same clear solubility trends as for wollastonite-I and are

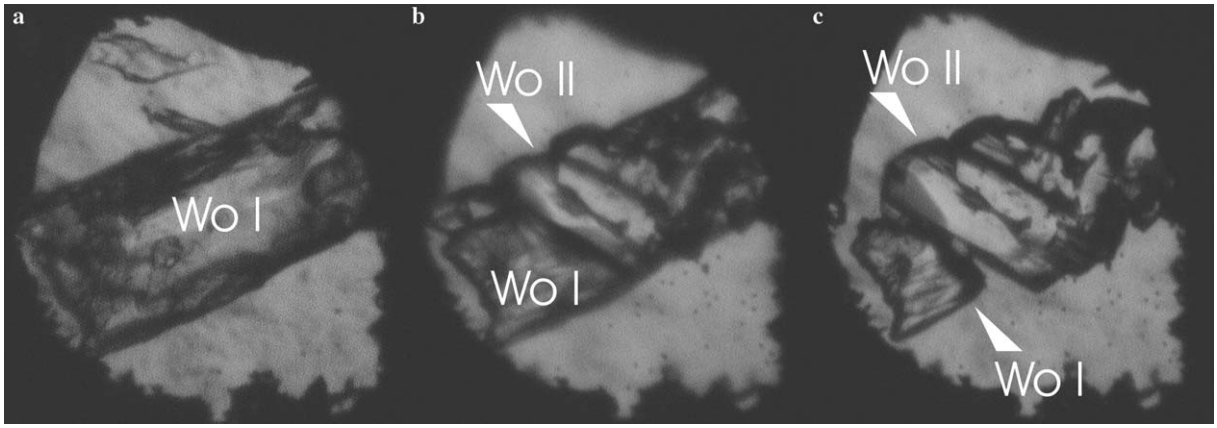

Fig. 3. Three stages in the progressive transformation of a wollastonite-I crystal to wollastonite-II in a diamond-anvil-cell experiment. The elapsed time between image (a) and (c) is less than one minute. The original wollastonite-I crystal is 300 μm in length.

not shown in Fig. 2. At 4.0 GPa the calculated solubility remains constant at approximately 6 wt% between 500 and 800 °C (Table 1). At 5.0 GPa the calculated solubility at 700 °C is 4 wt% and actually *lower* than the 10 wt% measured at 500 °C.

5. Discussion

The present study gives additional systematic insight into the solubility behaviour of a binary oxide that represents an important subsystem of many bulk compositions encountered in nature (e.g., calc-silicate rocks).

Fig. 2 shows that the solubility of wollastonite-I in pure water is positively correlated with both pressure and temperature. In the pressure–temperature range investigated, the molality of dissolved SiO_2 is always less than that for pure quartz (see summaries by Manning, 1994; Gerya et al., 2005), so that saturation and incongruent behaviour with respect to quartz should not be expected. An analogous comparison with the solubility of pure portlandite, $Ca(OH)_2$, is not possible, due to the lack of pertinent high-pressure/high-temperature data. Nevertheless, all other observations (e.g., direct DAC observation) in the present study indicate that wollastonite dissolution is congruent.

The data for wollastonite-II above 3.0 GPa are still too inconclusive to allow firm interpretation. The measured solubilities for wollastonite-II are lower than the extrapolated trends for wollastonite-I. This is compatible with phase theory. In addition, it is not unrealistic to expect that the very rapid reaction from wollastonite-I to wollastonite-II (Fig. 3) may have led to mechanical comminution of parts of the starting crystals. Thus the actual solubilities for wollastonite-II could be somewhat lower than the values determined by weight-loss.

In order to interpret the systematics of wollastonite-I solubility summarized in Fig. 2, a theoretical template is needed that goes beyond the simple linear fits shown there. A major problem in this regard is that the speciation of dissolved components at these high pressures is inadequately known. Although the work of Zotov and Keppler (2000, 2002), Zhang and Frantz (2000), Davis et al. (2001), Newton and Manning (2002, 2003) and Gerya et al. (2005) yields clear evidence that $Si(OH)_4$ silicon monomers will at higher pressures give way to more polymerized dimers and trimers, there are no corresponding unequivocal data for Ca. Both Ca^{2+} and $Ca(OH)^+$ species have been suggested to be important at low pressures of 0.1–0.2 GPa (e.g., Fein and Walther, 1987, 1989a; Xie and Walther, 1993b; Roselle and Baumgartner, 1995) and also up to 1.6 GPa (Caciagli and Manning, 2003), and it seems logical to speculate that the higher density and lower dielectric constant of the fluid at high pressures could result in an increasing importance of $Ca(OH)^+$ and $Ca(OH)_2$ species. Nevertheless, species containing both calcium and silicon must also be considered, especially at higher concentrations, temperatures and pressures. The general problem in characterizing high-pressure hydrous solutions is that in situ identification of dissolved species is still a zero-order problem (e.g., Doltsinis et al., 2004).

Successful approaches for modeling aqueous species and solubilities at low pressures via the modified Helgeson–Kirkham–Flowers equation of state (HKF EOS: e.g., Shock and Helgeson, 1988; Shock et al., 1989; Johnson et al., 1992; Tanger and Helgeson, 1998) are inherently not applicable at the high pressures above 0.5 GPa considered here, at which the density of water exceeds 1.0 g cm^{-3} (see discussion by Manning, 1994, 1998). However, it is known that the equilibrium constants of water dissociation and many other dissociation reactions correlate with the density of water such that $\log K$ is an isothermal linear function of $\log \rho(H_2O)$ (Marshall and Franck, 1981; Marshall and Mesmer, 1984; Eugster and Baumgartner, 1987; Mesmer et al., 1988; Anderson et al., 1991). Manning (1994, 1998) and Caciagli and Manning (2003) successfully extended this approach to at least 2 GPa for geologically relevant solutions and confirmed that, to a first approximation, the linear isothermal correlation between $\log K$ and $\log \rho(H_2O)$ holds. Even if speciations are thus not accurately known in our study, we expect that a density-based model should allow derivation of systematic trends in our experimental data set. We follow the formulation of Marshall and Franck (1981) and Manning (1994, 1998) and write

$$\log K = A + B \times T^{-1} + C \times T^{-2} + D \times T^{-3} + \log \rho(H_2O) \times (E + F \times T^{-1} + G \times T^{-2}), \quad (1)$$

with A through G being regressed constants. In keeping with the approach of Manning (1994) also used the equation of state for water of Halbach and Chatterjee (1982), which is valid up to 20 GPa and 1000 °C. For simplicity of formulation in the following section, we refer to ''wollastonite'' only, but ''wollastonite-I'' is always intended. In order to arrive at a simple equation describing our data together with the low-pressure runs of Xie and Walther (1993b), we optimized in various trial calculations between 4 and 7 parameters of Eq. (1), and found that at least 5 parameters are needed to describe the combined data set; the parameters D and G can be set to zero. Taking 6 or all 7 parameters of Eq. (1) into account in all cases yielded no significantly better optimizations. Although only data from 20 P-T coordinates are thus available for the 5-parameter regression at high pressures, this procedure appears justified, because the Xie and Walther (1993b) data at low pressure are fitted much better. All temperatures in this work are given in °C.

Lacking further information on speciation, we can write the dissolution reaction for wollastonite as

$$CaSiO_{3(solid)} = CaSiO_{3(aq)}. \quad (2)$$

Assuming an ideal dilute solution and setting the activity of solid wollastonite to unity allows setting $\log K$ equal to $\log(m_{woll})$, the logarithm of the molality of dissolved wollastonite.

The resulting fit is

$$\log(m_{\text{woll}}) = 2.2288 - 3418.23 \times T^{-1} + 671386.84 \times T^{-2} + \log \rho_{H_2O} \times (5.4578 + 2359.11 \times T^{-1}). \quad (3)$$

It is interesting to note that a number of experiments at 700 °C and 2 GPa (=$0.05\log(\rho_{H_2O})$) seem to deviate systematically toward lower values of solubility. A check of the original run protocols indicates that these are primarily runs QL-100 to QL-106 (Table 1), which were repeated in the same apparatus but at a much later time. Thus, a systematic error is indicated in these runs that could be identified on the basis of this density-based fit (see Fig. 4).

To provide an additional check on our data and the density-based fit, we have attempted to refine our results together with the experimental results of Xie and Walther (1993b) on the solubility of wollastonite + quartz at 0.2 GPa. Formulating the dissolution reaction as

$$\text{wollastonite}_{(\text{solid})} + \text{quartz}_{(\text{solid})} \rightarrow \text{CaO}_{(\text{aq})} + \text{SiO}_{2(\text{aq})} \quad (4)$$

the equilibrium constant can be defined as follows:

$$K_{\text{woll,qz}} = m_{\text{CaO(aq)}} \times m_{\text{SiO}_{2(\text{aq})}} / (a_{\text{wo}} \times a_{\text{qz}}), \quad (5)$$

where $m_{\text{CaO(aq)}}$ is the molality of CaO in the solution, $m_{\text{SiO}_{2(\text{aq})}}$ is the molality of SiO_2 in the solution, a_{wo} is the activity of wollastonite and a_{qz} is the activity of quartz. The activity of $\text{wollastonite}_{(\text{solid})}$ can be set to unity throughout. However, whereas the activity of $\text{quartz}_{(\text{solid})}$ can be set to unity in the quartz-saturated wollastonite + quartz experiments of Xie and Walther (1993b), this value must be calculated for our experiments by reference to the quartz-saturated SiO_2-H_2O solubility experiments of Manning (1994), which are formulated as an expression analogous to Eq. (3) above. Thus, assuming as a first approximation that the activity of water is unity,

$$\text{RTln}(m_{\text{SiO}_{2(\text{aq}),}}/a_{\text{qz},})_{\text{Manning}} = \text{RTln}(m_{\text{SiO}_{2(\text{aq})}}/a_{qz}) \quad (6)$$

$$\text{and} \quad a_{\text{qz}} = (a_{\text{qz,Manning}} \times m_{\text{SiO}_{2(\text{aq})}})/m_{\text{SiO}_{2(\text{aq}),\text{Manning}}}, \quad (7)$$

$K_{\text{wo,qz}}$ was then calculated for the available experimental data and for Eq. (3). Fig. 5a compares the isothermal linear fits obtained on the basis of only the high-pressure data of this study with the low-pressure, 0.2 GPa experimental data of Xie and Walther (1993b) between 301 and 661 °C. It is seen that the extrapolated isotherms based on the results of this study are reasonably close to the high-temperature, 0.2 GPa data points of Xie and Walther (1993b). However, with decreasing temperature, the data points predicted from our high-pressure experiments deviate increasingly from the experimental values of Xie and Walther (1993b).

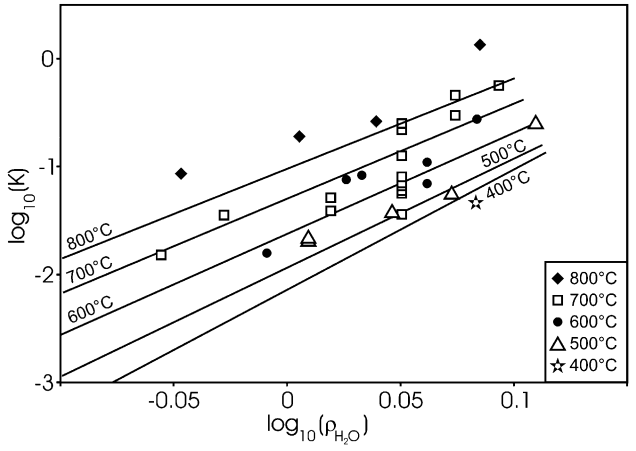

Fig. 4. Experimental results plotted in a $\log m_{\text{wo,qz}}$ vs. $\log \rho_{H_2O}$ diagram. The regressed isotherms are calculated from Eq. 3.

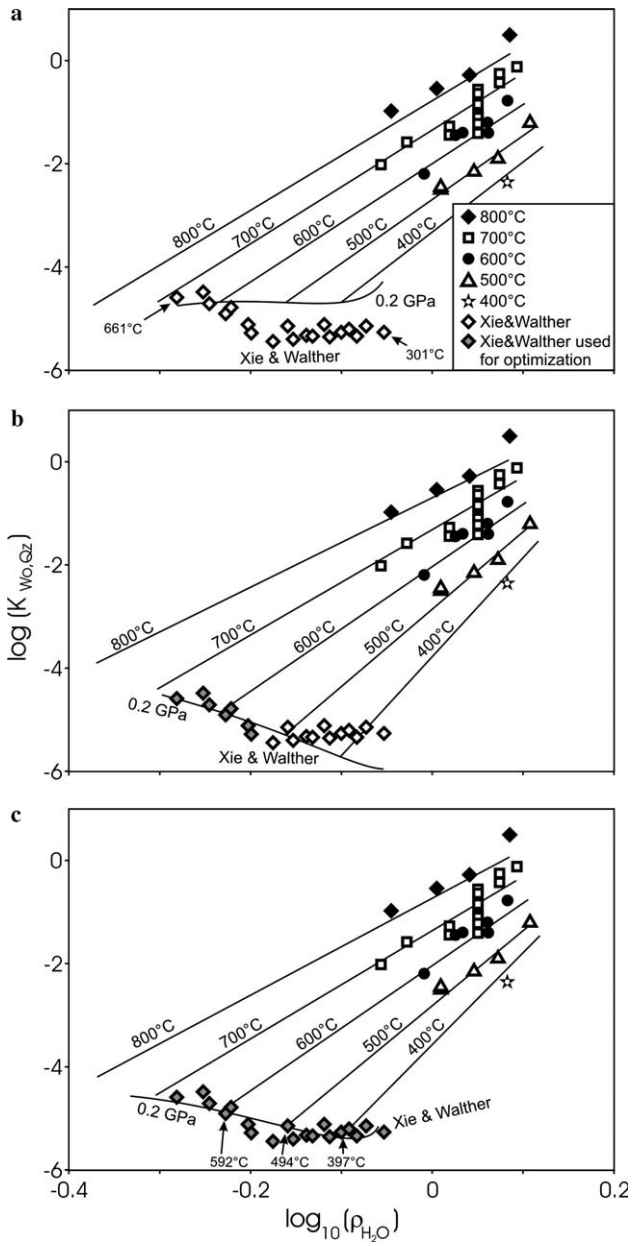

Fig. 5. $\text{Log}m_{\text{wo,qz}}$ vs. $\log \rho_{H_2O}$ diagrams successively combining the present data with experimental results on the solubility of wollastonite + quartz at 0.2 GPa (Xie and Walther, 1993b). See text for method of calculation. (a) Isothermal fits from the present study extrapolated to 0.2 GPa. (b) Isothermal fits combining present data with 0.2 GPa results at temperatures >550 °C. (c) Isothermal fits combining present data with all available 0.2 GPa data from Xie and Walther (1993b).

We then successively introduced the 0.2 GPa experimental data of Xie and Walther (1993b) into our own regressed high-pressure data set. Noting that the high-temperature data of Xie and Walther (1993b) fit our experimental data best, and also that there is a marked discontinuity in the Xie and Walther data trend at 550 °C, we introduced the Xie and Walther data in two steps. Fig. 5b indicates the change in the regressed isotherms when only the high-temperature (i.e., >550 °C) data of Xie and Walther (1993b) are considered. The corresponding fitted polynomial analogous to Eq. (3) changes to

$$\log(m_{\mathrm{woll}}) = 2.1075 - 2989.10 \times T^{-1} + 448894.38 \times T^{-2} + \log \rho_{\mathrm{H_2O}} \times (-4.0399 + 8373.33 \times T^{-1}). \quad (8)$$

Fig. 5c shows the results obtained when all experimental data from the present study and from Xie and Walther (1993b) are combined and regressed together. Eq. (3) then modifies to

$$\log(m_{\mathrm{woll}}) = 2.5930 - 3660.98 \times T^{-1} + 671402.32 \times T^{-2} + \log \rho_{\mathrm{H_2O}} \times (-1.3609 + 6775.13 \times T^{-1}). \quad (9)$$

The differences between the introduction of either a partial or the whole experimental data set from Xie and Walther (1993b) is relatively small. However, it is clear from Fig. 5c that the approach outlined above returns values that fit the Xie and Walther (1993b) experimental data well. The combined regression of this data with the high-pressure experimental results of the present study leads to a marked rotation of the isothermal linear fits. Considering the scatter in the high-pressure data, these fits must still be deemed acceptable. At 25 °C and 1 bar, Eq. (9) leads to a logarithm of the equilibrium constant of −6.7, which appears realistic when compared to the value of −4.0 for quartz solubility at these conditions (Manning, 1994). Calculations with the computer program SUPCRT92 (Johnson et al., 1992) using the only equation possible in the given data set for the solubility of wollastonite in water:

$$CaSiO_3 + H_2O = SiO_{2(aq)} + Ca^{2+} + 2OH^- \quad (10)$$

yield $\log K = -14.1$.

This very low equilibrium constant is not reproduced by the experiments, which demonstrate a clearly lower solubility of wollastonite compared to quartz but only 10 times lower. This suggests that the speciation of calcium in our system is probably not or not only Ca^{2+}, and that other or additional species should be present in the fluid at high P-T conditions.

Thus, given the present lack of unequivocal knowledge on Ca speciation at both low and high pressures, a H_2O-density-based approximation (Manning, 1994, 1998; Caciagli and Manning, 2003) such as represented by Eq. (9) can be considered to be an adequate description of the absolute solubility of wollastonite in quartz-saturated solutions from 0.2–3 GPa to 300–800 °C.

Acknowledgments

This study was supported by the German Science Foundation within the framework of the Collaborative Research Center (Sonderforschungsbereich) 526 "Rheology of the Earth." The authors thank G. Andersen for maintaining the high-pressure equipment in excellent working condition. H.-J. Bernhardt and R. Neuser helped in performing difficult chemical analyses and in characterizing the run products. J. Gross and K. Klevakina patiently assisted in the difficult preparation of gold capsules. J.V. Walther provided valuable discussion in an earlier stage of this project.

Associate editor: David J. Wesolowski

References

Anderson, G.M., Castet, S., Schott, J., Mesmer, R.E., 1991. The density model for estimation of thermodynamic parameters of reactions at high temperatures and pressures. *Geochim. Cosmochim. Acta* **55**, 1769–1779.

Bailey, A., Reesman, A.L., 1971. A survey study of the kinetics of wollastonite dissolution in H_2O-CO_2 and buffered systems at 25 °C. *Am. J. Sci.* **271**, 464–472.

Becker, K.H., Cemič, L., Langer, K.E., 1983. Solubility of corundum in supercritical water. *Geochim. Cosmochim. Acta* **47**, 1573–1578.

Burchard, M., Zaitsev, A.M., Maresch, W.V., 2003. Extending the pressure and temperature limits of hydrothermal diamond anvil cells. *Rev. Sci. Instrum.* **74**, 1263–1266.

Caciagli, N., Manning, C.E., 2003. The solubility of calcite in water at 6–16 kbar and 500–800 °C. *Contrib. Mineral. Petrol.* **146**, 275–285.

Casey, W.H., Westrich, H.R., Banfield, J.F., Ferruzzi, G., Arnold, G.W., 1993. Leaching and reconstruction at the surface of dissolving chain-silicate minerals. *Nature* **366**, 253–256.

Davis, M.K., Fumagalli, P., Stixrude, L.P., 2001. Thermodynamics of silicate dissolution from in-situ Raman spectroscopy. *Eos. Trans. AGU* **82** (47), Fall. Meet. Suppl., Abstract T31C-0860.

Doltsinis, N.L., Burchard, M., Maresch, W.V., 2004. Ab initio molecular dynamics simulations as a tool for interpreting vibrational spectra in aqueous fluids. In: *EMPG-X Symposium Abstracts. Lithos*, **73** (Suppl.), S28.

Eggler, D.H., Rosenhauer, M., 1978. Carbon dioxide in silicate melts: II. Solubilities of CO_2 and H_2O in $CaMgSi_2O_6$ (Diopside) liquids and vapors at pressures to 40 kb. *Am. J. Sci.* **278**, 64–94.

Eugster, H.P., Baumgartner, L., 1987. Mineral solubilities and speciation in supercritical metamorphic fluids. In: Carmichael, I.S.E., Eugster, H.P. (Eds), *Thermodynamic Modeling of Geologic Materials: Minerals, Fluids, and Melts. Rev. Mineral.* **17**, 367–403.

Fein, J.B., Walther, J.V., 1987. Calcite solubility in supercritical CO_2-H_2O fluids. *Geochim. Cosmochim. Acta* **51**, 1665–1673.

Fein, J.B., Walther, J.V., 1989a. Calcite solubility and speciation in supercritical NaCl-HCl aqueous fluids. *Contrib. Mineral. Petrol.* **103**, 317–324.

Fein, J.B., Walther, J.V., 1989b. Portlandite solubilities in supercritical Ar-H_2O mixtures: implications for quantifying solvent effects. *Am. J. Sci.* **289**, 975–993.

Fockenberg, T., 1998. An experimental study of the pressure-temperature stability of MgMgAl-pumpellyite in the system MgO-Al_2O_3-SiO_2-H_2O. *Am. Mineral.* **83**, 220–227.

Franz, J.D., Popp, R.K., Boctor, N.Z., 1981. Mineral-solution equilibria—V. Solubilities of rock-forming minerals in supercritical fluids. *Geochim. Cosmochim. Acta* **45**, 69–77.

Gerya, T.V., Maresch, W.V., Burchard, M., Zakhartchouk, V., Doltsinis, N.L., Fockenberg, T., 2005. Thermodynamic modeling of solubility and speciation of silica in H_2O-SiO_2 fluid up to 1300 °C and 20 kbar based on the chain reaction formalism. *Eur. J. Mineral.* **17**, 269–283.

Gunter, W.D., Eugster, H.P., 1978. Wollastonite solubility and free energy of supercritical aqueous $CaCl_2$. *Contrib. Mineral. Petrol.* **66**, 271–281.

Halbach, H., Chatterjee, N.D., 1982. An empirical Redlich-Kwong-type equation of state for water to 1000 °C and 200 kbar. *Contrib. Mineral. Petrol.* **79**, 337–345.

Huang, W.-L., Wyllie, P.J., 1975. Melting and subsolidus relationships for $CaSiO_3$ to 35 kbars pressure. *Am. Mineral.* **60**, 213–217.

Johnson, J.W., Oelkers, E.H., Helgeson, H.C., 1992. SUPCRT92: a software package for calculating the standard molal thermodynamic properties of minerals, gases, aqueous species, and reactions from 1 to 5000 bar and 0 to 1000 °C. *Comput. Geosci.* **18**, 899–947.

Manning, C.E., 1994. The solubility of quartz in H_2O in the lower crust and upper mantle. *Geochim. Cosmochim. Acta* **58**, 4831–4839.

Manning, C.E., 1998. Fluid composition at the blueschist-eclogite transition in the model system Na_2O-MgO-Al_2O_3-SiO_2-H_2O-HCl. *Schweiz. Mineral. Petrogr. Mitt.* **78**, 225–242.

Manning, C.E., 2004. The chemistry of subduction-zone fluids. *Earth Planet. Sci. Lett.* **223**, 1–16.

Manning, C.E., Boettcher, S.L., 1994. Rapid-quench hydrothermal experiments at mantle pressures and temperatures. *Am. Mineral.* **79**, 1153–1158.

Marshall, W.L., Franck, E.U., 1981. Ion product of water substance, 0–1000 °C, 1–10,000 bar. New international formulation and its background. *J. Phys. Chem. Ref. Data* **10**, 295–304.

Marshall, W.L., Mesmer, R.E., 1984. Pressure-density relationships and ionization equilibria in aqueous solutions. *J. Soln. Chem.* **13**, 383–391.

Mesmer, R.E., Marshall, W.L., Palmer, D.A., Simonson, J.M., Holmes, H.F., 1988. Thermodynamics of aqueous association and ionization reactions at high temperatures and pressures. *J. Soln. Chem.* **17**, 699–718.

Newton, R.C., Manning, C.E., 2000. Quartz solubility in H_2O-NaCl and H_2O-CO_2 solutions at deep crust-upper mantle pressures and temperatures: 2–15 kbar and 500–900 °C. *Geochim. Cosmochim. Acta* **64**, 2993–3005.

Newton, R.C., Manning, C.E., 2002. Solubility of enstatite + forsterite in H_2O at deep crust/upper mantle conditions: 4 to 15 kbar and 700 to 900 °C. *Geochim. Cosmochim. Acta* **66**, 4165–4176.

Newton, R.C., Manning, C.E., 2003. Activity coefficient and polymerization of aqueous silica at 800 °C, 12 kbar, from solubility measurements on SiO_2-buffering mineral assemblages. *Contrib. Mineral. Petrol.* **146**, 135–143.

Popp, R.K., Frantz, J.D., 1979. Mineral solution equilibria II: an experimental study of mineral solubilities and the thermodynamic properties of aqueous $CaCl_2$ in the system CaO-SiO_2-H_2O-HCl. *Geochim. Cosmochim. Acta* **43**, 1777–1790.

Rimstidt, J.D., Dove, P.R., 1986. Mineral/solution reaction in a mixed flow reactor: wollastonite hydrolysis. *Geochim. Cosmochim. Acta* **50**, 2509–2516.

Roselle, G.T., Baumgartner, L.P., 1995. Experimental determination of anorthite solubility and calcium speciation in supercritical chloride solutions at 2 kb and 400 to 600 °C. *Geochim. Cosmochim. Acta* **59**, 1539–1549.

Seewald, J.S., Seyfried Jr., W.E., 1991. Experimental determination of portlandite solubility in H_2O and acetate solutions at 100–350 °C and 500 bars: constraints on calcium hydroxide and calcium acetate complex stability. *Geochim. Cosmochim. Acta* **55**, 659–669.

Shock, E.L., Helgeson, H.C., 1988. Calculation of the thermodynamic and transport properties of aqueous species at high pressures and temperatures: correlation algorithms for ionic species and equation of state predictions to 5 kb and 1000 °C. *Geochim. Cosmochim. Acta* **52**, 2009–2036.

Shock, E.L., Helgeson, H.C., Sverjensky, D.A., 1989. Calculation of the thermodynamic and transport properties of aqueous species at high pressures and temperatures: standard partial molal properties of inorganic neutral species. *Geochim. Cosmochim. Acta* **53**, 2157–2183.

Tanger, J.C., Helgeson, H.C., 1998. Calculation of the thermodynamic and transport properties of aqueous species at high pressures and temperatures: revised equation of state for the standard partial molal properties of ions and electrolytes. *Am. J. Sci.* **288**, 19–98.

Trojer, F.J., 1969. The crystal structure of a high pressure form of $CaSiO_3$. *Z. Kristallogr.* **130**, 185–206.

Walther, J.V., 1986. Experimental determination of portlandite and brucite solubilities in supercritical H_2O. *Geochim. Cosmochim. Acta* **50**, 733–739.

Weissbart, E.J., Rimstidt, J.D., 2000. Wollastonite: incongruent dissolution and leached layer formation. *Geochim. Cosmochim. Acta* **64**, 4004–4016.

Xie, Z., Walther, J.V., 1993a. Quartz solubilities in NaCl solutions with and without wollastonite at elevated temperatures and pressures. *Geochim. Cosmochim. Acta* **57**, 1947–1955.

Xie, Z., Walther, J.V., 1993b. Wollastonite + quartz solubility in supercritical NaCl aqueous solutions. *Am. J. Sci.* **293**, 235–255.

Xie, Z., Walther, J.V., 1994. Dissolution stoichiometry and adsorption of alkali and alkaline earth elements to the acid-reacted wollastonite surface at 25 °C. *Geochim. Cosmochim. Acta* **58**, 2587–2598.

Zaitsev, A.M., Burchard, M., Meijer, J., Stephan, A., Burchard, B., Fahrner, W.R., Maresch, W., 2001. Diamond pressure and temperature sensors for high-pressure high-temperature applications. *Phys. Stat. Sol.* **185**, 59–64.

Zhang, Y.-G., Frantz, J.D., 2000. Enstatite-forsterite-water equilibria at elevated temperatures and pressures. *Am. Mineral.* **85**, 918–925.

Zotov, N., Keppler, H., 2000. In-situ Raman spectra of dissolved silica in aqueous fluids to 900 °C and 14 kbar. *Am. Mineral.* **85**, 600–604.

Zotov, N., Keppler, H., 2002. Silica speciation in aqueous fluids at high pressures and high temperatures. *Chem. Geol.* **184**, 71–82.